



The fracture toughness of polymer cellulose nanocomposites using the essential work of fracture method

M. Shir Mohammadi¹, C. Hammerquist¹, J. Simonsen¹, and J. A. Nairn^{1,*} 

¹ Wood Science and Engineering, Oregon State University, 112 Richardson Hall, Corvallis, OR 97330, USA

Received: 29 March 2016

Accepted: 15 June 2016

Published online:
29 June 2016

© Springer Science+Business
Media New York 2016

ABSTRACT

This work reinforced both a glassy polymer (high stiffness matrix) and a rubbery polymer (low stiffness matrix) with cellulose nanocrystals (CNC) derived from natural sources. CNC addition always increased stiffness while it increased toughness for a rubbery polymer and caused no loss in toughness for a glassy polymer. These results contradict many claims that when stiffness increases, the toughness decreases. We show that these claims depend on how toughness is measured. Our results were based on toughness measured using the essential work of fracture method. In contrast, toughness determined from area under the stress–strain curve shows a significant decrease, but that method may be a poor measure of toughness. Property enhancements usually require a good fiber/matrix interface. We used modeling of stiffness properties to confirm that CNC has a good interface with the studied polymer matrices.

Introduction

Nanofillers are often used to increase polymer mechanical properties, such as modulus, yield strength, ultimate strength [5, 22], ductility [35], and toughness [32]. Measuring nanocomposite toughness, however, can be a challenge. Some studies use total work of fracture (W_f defined as area under the stress–strain curve) to measure “toughness” [9, 30, 35, 39]. Our view is that W_f is not a material property and therefore not an ideal indicator of toughness. Instead, toughness should be associated with the amount of energy required to extend an existing crack by a unit amount of area [1].

Crack extension toughness can be measured by critical stress intensity factor, K_c , or by energy required to propagate a crack, G_c . These experiments are commonly done in opening or mode I because mode I K_c and G_c are usually the lowest toughnesses and therefore a critical test in nanocomposites for the role of fillers on toughness properties. Measurement of mode I K_c requires specialized specimens while G_c can be measured on any specimen by directly measuring energy released as a function of crack growth [3, 14, 21, 36]. If either one can be measured, the other can be calculated by the relations:

Address correspondence to E-mail: John.Nairn@oregonstate.edu

$$K_c = \sqrt{\frac{G_c E}{1 - \nu^2}} \quad (\text{if plane strain}), \tag{1}$$

$$K_c = \sqrt{G_c E} \quad (\text{if plane stress}), \tag{2}$$

where E is Young’s modulus in the applied stress direction and ν is Poisson’s ratio. Under plane strain conditions K_c and G_c are usually called K_{Ic} and G_{Ic} and are material properties. In plane stress conditions, K_c and G_c are still useful, but may depend on specimen thickness.

The fracture toughness of brittle polymer nanocomposites (e.g., epoxy/carbon nanotube) has been measured using both impact tests (a K_c method) [6] and crack propagation (a G_c method) [16]. These tests show that nanofiller addition increases fracture toughness provided the interface between fibers and the matrix is good [41] and the nanofillers are well dispersed [6]. The experiments here used thin nanocomposite films, which is a common form for making nanocomposites. Unfortunately, typical impact or crack propagation tests do not work for thin nanocomposite films, especially films derived using ductile polymers. Impact tests do not work for films and it can be difficult to objectively record crack propagation as well. Some alternate methods are needed for thin films.

Because work of fracture (W_f) experiments are easy and avoid the need to monitor crack propagation, it is tempting to resort to such tests. In brief, W_f is defined as total work per unit specimen area to break an unnotched specimen. It is found from area under the stress–strain curve:

$$W_f = \frac{1}{Wt} \int F dx = L \int \sigma d\varepsilon, \tag{3}$$

where W , t , and L are specimen width, thickness, and length, F is applied force, x is displacement, σ is applied stress, and ε is strain. Because final failure must be associated with crack initiation and propagation across the specimen, one could speculate that W_f is an average of the crack propagation fracture toughness for crack growth from zero to W or

$$W_f = \frac{1}{W} \int_0^W G_c dx = G_c \tag{4}$$

and equality of W_f with G_c assumes G_c is constant. Unfortunately, many influences, such as crack initiation, edge effects, and energies not associated with crack propagation, cause W_f to only be crudely

related to G_c . When W_f was used to characterize nanocellulose-reinforced nanocomposites, the general trend was that stiffness increases but W_f decreases as filler content increases [7, 18, 30, 38]. As a result, a consensus has emerged that nanofiller addition decreases the toughness of polymers [10, 30]. This consensus derived from W_f experiments may be misleading and might change by switching to improved methods for measuring toughness.

For ductile polymers and films, an alternate fracture method, known as the essential work of fracture method (EWFm), has been advocated [4, 19, 20, 33, 34]. In brief, the EWFm measures specific work of fracture (total work of fracture per unit ligament area denoted here using lower case w_f) for a series of deep, double-edge notched specimens tested in tension (Fig. 1). The total specific work of fracture for a given ligament length, ℓ , is partitioned into plastic work per unit volume, w_p , which is confined to a plastic zone in the ligament zone (of length ℓ), and an essential work of fracture per unit area, w_e , associated with crack propagation. The specific work of fracture becomes

$$w_f = w_e + \beta w_p \ell \quad \text{where} \quad w_f = \frac{1}{\ell t} \int F dx \tag{5}$$

and β is a factor describing the plastic zone shape (e.g., elliptical, circular, etc.) [19]. The experiments are to measure w_f as a function of ℓ . These results are typically linear with slope equal to βw_p and intercept equal to w_e . Both these properties provide useful material properties (although they may depend on thickness [4]). The slope is related to ductility while the intercept characterizes the plane stress fracture toughness of the film or measures G_c . The EWFm combines the ease of work of fracture experiments (except it needs multiple specimens) with a fracture mechanics result for toughness (w_e). The method avoids initiation effects (by cutting notches) and edge effects (using deep notches). It avoids the need to measure crack growth in ductile materials by using multiple specimens with different ligament lengths (the ligament length becomes total amount of crack propagation for each specimen). Importantly, the slope and intercept from EWFm separates plastic energy dissipation not associated with crack growth (βw_p) from inherent toughness or energy required to propagate a crack (w_e). This separation contrasts with W_f experiments where these two effects are combined

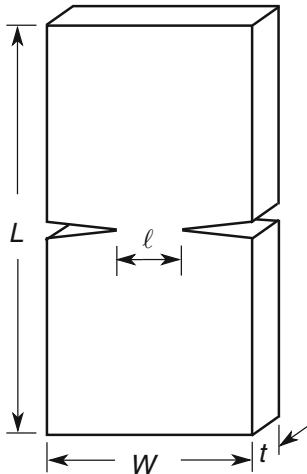


Figure 1 Deep, double-edged, notched specimens (DDENT) tested in tension for EWFM experiments.

with unknown proportions. More details about the EWFM can be found elsewhere [1, 4, 19, 20, 33, 34].

We studied reinforcement of two different polymers with cellulose nanocrystals (CNC)—poly(vinylidene fluoride-co-hexafluoropropylene) (PVdF-HFP) and polysulfone (PSF). Experiments show that PVdF-HFP and PSF both are compatible with CNC and the addition of CNC significantly increased their stiffness [12, 13]. For toughness properties, we compared traditional W_f test methods to the EWFM. Although W_f declined significantly with added CNC, the essential work of fracture, w_e , which we claim is a more rigorous measure of toughness, showed the toughness increased for PVdF-HFP and remained about the same for PSF. For both polymers, the ductility decreased and that decrease was reflected in decreased βw_p . Additional studies used modeling to quantify interfacial properties and reanalyzed fracture data to evaluate the role of thickness when interpreting EWFM experiments.

Materials and methods

Materials

Sulfonate CNC (S-CNC) dispersed in water (11 % solids) was purchased from the University of Maine. Dimethylacetamide (DMAc) was used as the organic solvent and it was purchased from Honeywell Burdick & Jackson Co., MI, USA. The rubbery polymer, PVdF-HFP, with molecular weight of 400,000 D and

density of 1.78 g/cm^3 was purchased from Aldrich Chemical Co. The glassy polymer, polysulfone (PSF) with a molecular weight of 35,000 D and density of 1.24 g/cm^3 , was donated by Solvay Advanced Polymers (Alpharetta, GA, USA).

Nanocomposite fabrication

DMAc was added to a CNC/water solution to reach 4 % CNC in DMAc (note this % content and all others in this paper are percent contents by weight). A Rotavapor (Büchi RE111, Switzerland) was used to completely evaporate water from the solution (PSF and PVdF-HFP do not dissolve in water). PVdF-HFP was dissolved in DMAc and was mixed with the dispersed CNC in DMAc to reach the desired CNC weight content in the PVdF-HFP composite and stirred for 0.5 h at $85 \text{ }^\circ\text{C}$ to yield a uniform solution. The total solution solids were $\sim 5 \%$. The same procedure was used for the PSF composites.

Centrifugal casting was used to cast films in order to reduce the trapped solvent and to get uniform thickness. In centrifugal casting, a solution is poured into a metal beaker that is attached to a motor. Then the beaker is partially sealed with a center-hole cap to contain the liquid, but allow solvent evaporation. The beaker is rotated at 1800 rpm and films are cast on the beaker wall. A heat gun is applied to the exterior of the metal beaker to control the temperature. All films were cast at $70\text{--}80 \text{ }^\circ\text{C}$.

Mechanical testing

All samples were cut to 12.7 mm width and 40 mm length. The thickness of the cast films varied within and between films. We therefore measured each film's thickness using an optical microscope (Nikon Eclipse E400) and it ranged from 20 to $80 \text{ }\mu\text{m}$. All samples were tested at room temperature using an Instron 4301 with a 100 N load cell capacity and the gage length was 20 mm. The crosshead speed was set to 1 mm/min for PVdF-HFP films. But for PSF films, due to their glassy nature, a 0.5 mm/min rate was chosen in order to reach the plastic region prior to failure. Stress–strain curves were calculated by dividing the force by the initial cross-sectional area and displacement by the initial gage length. Young's modulus was calculated from initial slope of the stress–strain curves (up to about 0.1 % strain). Offset yield stress (σ_Y) was determined by finding the

intersection of a line having the initial slope of the stress–strain curve but offset by 1 % strain from that curve.

Essential work of fracture experiments

EWFM experiments used DDENT specimens (Fig. 1). Mirrored notches were cut at the centerline of the samples using a razor blade. The notch depths were varied such that the remaining ligament lengths (ℓ) varied from 0.5 to 3.5 mm. Because our maximum thickness was $t = 80 \mu\text{m}$ and specimen widths were $W = 12.7 \text{ mm}$, all specimens were confined to the recommended range of $3t < \ell < W/3$ for measuring plane stress essential work of fracture [19]. Samples were loaded in tension and stress–strain curves were measured up to failure. Afterwards, the specific work of fracture (w_f) was plotted as a function of ligament length (ℓ). Ductility was measured from the slope and essential work of fracture was calculated by extrapolating the curve to $\ell = 0$.

Results and discussion

Tensile tests on unnotched specimens

Figure 2 (top) shows the mechanical testing results for unnotched films of both pure PVdF-HFP polymer and of PVdF-HFP/15 % CNC nanocomposites. The yield strength, σ_Y , of PVdF-HFP with the addition of 15 % CNC increased ~ 2 times, the maximum strength, σ_{UTS} , increased ~ 30 %, and the modulus increased ~ 3 times. Fig 2 (bottom) shows that these same properties also increased from PSF to PSF/15 % CNC nanocomposites— σ_Y and σ_{UTS} increased slightly (although not a significant increase) while the modulus increased 80 %. But most PSF/15 % CNC films broke before 1 % deformation meaning we could not measure yield strength (because the stress–strain curve did not reach the 1 % offset line). For these films yield strength was assumed the same as σ_{UTS} .

These increases all suggested that both PVdF-HFP and PSF are compatible with added CNC and the fibers were well dispersed. Visual inspection of the films supported this claim. The increases, especially in ultimate strengths, also suggest that the CNCs did not introduce any flaws into the polymer (point of weakness for failure). Nevertheless, the total fracture

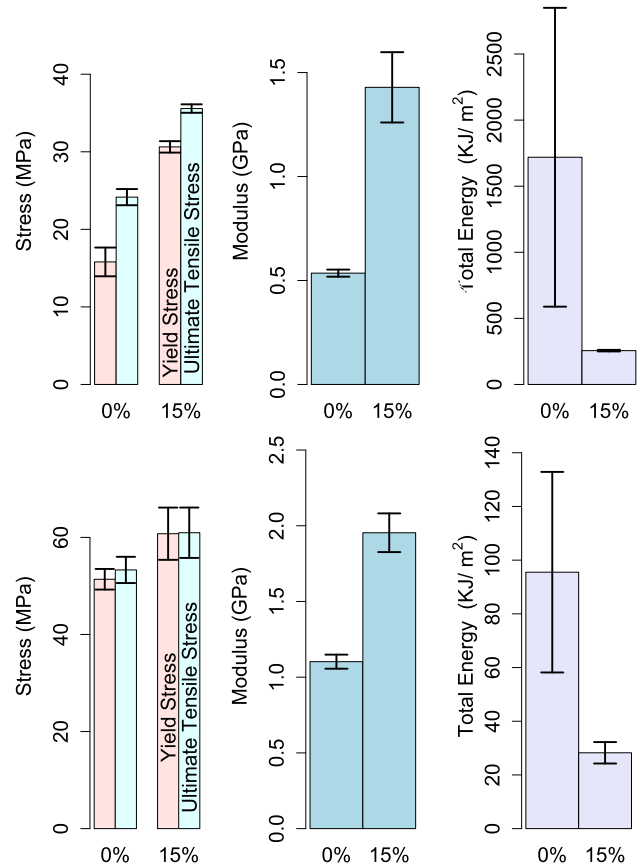


Figure 2 Mechanical testing results from stress–strain curves for nanocomposite films. *Top* PVdF-HFP and PVdF-HFP/15 % CNC films. *Bottom* PSF and PSF/15 % CNC films.

energy, W_f , for PVdF-HFP films decreased 85 % with the addition of 15 % CNC, while for PSF films, W_f decreased by 70 %. But, does a decrease in W_f mean their toughness has decreased?

Essential work of fracture experiments

Figure 3 (top) shows EWFM results on notched specimens for w_f as a function of ligament length (ℓ) for both PVdF-HFP and PVdF-HFP/15 % CNC nanocomposite films. Note that most EWFM experiments use constant film thickness, but for these films, it was difficult to control thickness. We therefore included results for all thicknesses in the EWFM plots. The variations in thickness may have contributed to scatter in results, but such thickness effects are addressed in more detail below. The slope of EWFM results (βw_p) decreased from pure PVdF-HFP films to CNC nanocomposite indicating a reduction in plastic ductility. For 15 % CNC films, the

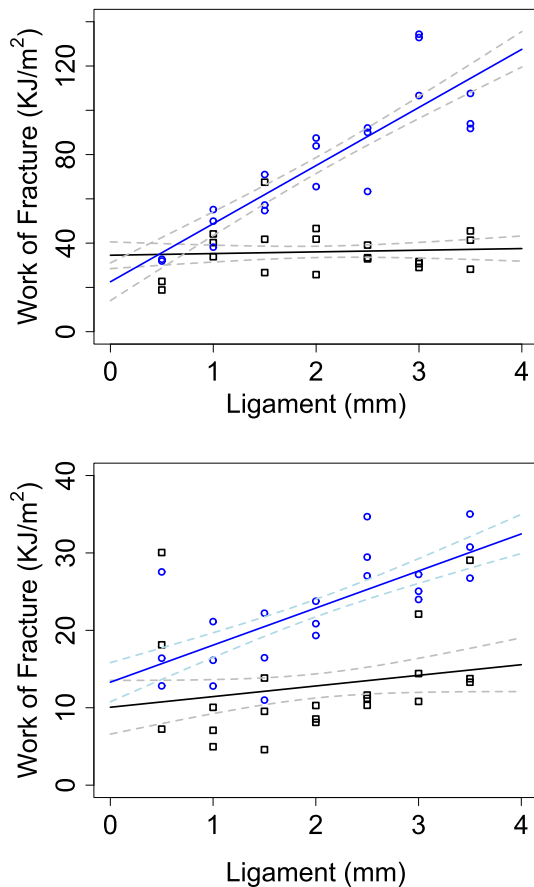


Figure 3 Work of fracture w_f vs. ligament (ℓ) plots to find the essential work of fracture (w_e). Top PVdF-HFP (circle) and PVdF-HFP/15 % CNC (Square). Bottom PSF (circle) and PSF/15 % CNC (square). Dashed lines represent ± 1 standard error for the linear fit.

slope, was close to zero with only a slight increase with increasing ligament length. Extrapolation to zero ligament length gave essential work of fracture for pure films of $w_e = 22.5 \pm 8.3 \text{ kJ/m}^2$. For 15 % CNC films, the toughness increased to $w_e = 34.5 \pm 5.2 \text{ kJ/m}^2$ (the uncertainties are ± 1 standard error for the linear fit). For PSF [Fig. 3 (bottom)], the addition of 15 % CNC decreased the slope (βw_p), which was consistent with observation that CNC made the PSF less deformable. CNC addition changed toughness from $w_e = 13.3 \pm 2.5 \text{ kJ/m}^2$ for pure PSF to $w_e = 10.1 \pm 3.4 \text{ kJ/m}^2$ for PSF/15 % CNC, but this change was not significant within one standard error (± 68 % confidence).

Contrary to the dramatic drop in W_f for unnotched films, the toughness as measured by w_e increased with CNC addition for PVdF-HFP and caused little or

no decrease for PSF. The proponents of EWFM [4, 19] contend that w_e is a better measure of toughness than W_f . In our films the drop in W_f was likely caused by loss of ductility rather than inherent toughness. When toughness is separated from ductility, CNC addition increases the toughness of PVdF-HFP films. Even in PSF where no increase was observed, the fact that toughness did not decrease suggests that the CNC addition has enhanced toughness enough to overcome the overall decrease in ductility. If we assume that the polymer structure does not change with CNC addition, the increase in the fracture toughness suggests good interfacial properties and a sufficient filler density to retard crack propagation.

Interface modeling

One way to validate interface quality, as suggested by enhanced properties above, is to compare the observed increase in modulus to theoretical predictions for a short fiber composite modulus using a model that accounts for interfacial properties. Nairn and Shir Mohammadi [24] recently developed an enhanced shear lag model for short fiber composites that explicitly models imperfect interfaces on both the fiber sides and the fiber ends. It is called the end-capped shear lag model. The interface is modeled using interfacial stiffness terms— $r_f D_n$ and $r_f D_t$ —where r_f is the fiber radius and D_n and D_t are imperfect interface parameters for normal and tangential loading that vary from 0 for a debonded interface to ∞ for a perfect interface [8]. Although the end-capped model was verified by comparison to numerical models, it has two problems. As introduced, the model only applies for aligned short fiber composites and like all other numerical and analytical models, it degenerates to a lower bound result when the fiber to matrix modulus ratio gets high (>100). The Appendix describes the model and extends it to handle both randomly oriented composites and composites with soft matrices. This section applies the extended model to the current experiments.

If all material properties are known except the interfacial properties, modeling calculations can give information about the interface. The CNC fibers used here were estimated to have modulus $E_f = 105 \text{ GPa}$ [23], Poisson's ratio $\nu_f = 0.28$, aspect ratio $\rho = 18$, and diameter $r_f = 10 \text{ nm}$. For PSF, the matrix properties

were measured or estimated as modulus $E_m = 1.2$ GPa and Poisson's ratio $\nu_m = 0.33$. For this material, the fiber to matrix modulus ratio is $R = E_f/E_m = 87.5$. Because $R < 100$, the properties can be calculated using the end-capped shear lag model (see Appendix). If the interfaces are assumed perfect ($r_f D_n = r_f D_t = \infty$) the calculated composite modulus with 15 % fibers is 2.9 GPa, which is above the measured result of 1.8–2.0 GPa (see Fig. 2). If we assume the difference is caused by imperfect interfaces, the experimental result can be fit by setting $r_f D_n = r_f D_t = 250$ MPa.

For PVdF-HFP, the matrix properties were measured or estimated as modulus $E_m = 0.55$ GPa and Poisson's ratio $\nu_m = 0.33$. For this material, the fiber to matrix modulus ratio is $R = E_f/E_m = 190$. Because $R > 100$, the properties can be calculated using shear lag model calibrated for soft matrices that add 93 % of the end-capped model with 7 % of a fiber effectiveness method (see Appendix). In this model the PVdF-HFP composite with 15 % CNC and perfect interfaces is predicted to have modulus of 2.3 GPa. The experimental results can be fit by adjusting the interface parameters to $r_f D_n = r_f D_t = 350$ MPa.

These calculations show that the interface properties for PSF and PVdF-HFP are similar to PVdF-HFP perhaps having a slightly better interface. Because these interface parameters are difficult to measure, there are few results to help decide what values constitute a "good" interface. Some previous results for carbon/epoxy used Raman methods to directly observe stress transfer into the fiber and the results could be fit to determine interface parameters [29]. The result for sized carbon fibers with a known good interface had $r_f D_t = 300$ MPa. By analogy, the CNC composite here can be characterized as having good interfaces. More details about fitting nanocomposite experiments with interface properties will be reported in a future publication [37].

Fractography

Although fillers can reduce ductility (as observed by slope of EWFM experiments), when viewed as energy per increment of crack growth, fillers can block crack propagation and increase toughness (as shown schematically in Fig. 4). For this mechanism to be effective, there needs to be a good interfacial bond between matrix and fibers and enough fibers to

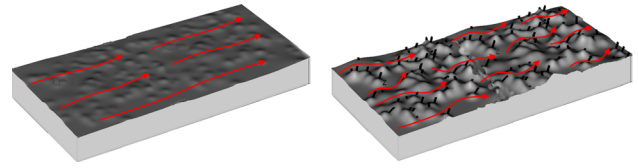


Figure 4 Schematic picture of fracture surface of polymers (left) and polymer nanocomposite (right).

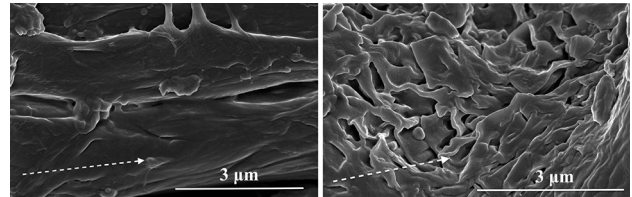


Figure 5 Fracture surface of PVdF-HFP (left) and PVdF-HFP/15 % CNC (right). Arrows show the crack propagation direction.

inhibit crack growth. A weak interface causes fiber pull-out and is less effective at inhibiting crack propagation. Too few fibers decreases the probability of blocking the crack.

To look for evidence of these mechanisms in our composites, we used fractography of the fracture surfaces for pure polymer and for CNC composites. Figure 5 shows scanning electron microscopy (SEM) images of the fracture surface for both pure PVdF-HFP and PVdF-HFP/15 % CNC. In pure PVdF-HFP the crack surface is smooth with straight propagation. In contrast, with 15 % CNC the crack was not straight and the surface was rough, presumably because propagation was deflected by the CNCs. In other words, CNC addition to the polymer gave a local increase in the fracture energy as the crack propagated more through the weaker areas and thus deviated from straight crack propagation. Such a crack path may explain the observed increase in the essential work of fracture. Lin et al. [17] showed similar crack deviation behavior in polypropylene filled with 20 % CaCO_3 nanoparticles and saw an increase in fracture toughness (as measured by impact tests).

SEM images of fracture surfaces for pure PSF and PSF/15 % CNC films show some similarities and some differences (Fig. 6). In pure PSF, like pure PVdF-HFP, the crack propagation is clear and straight. The addition of 15 % CNC (Fig. 6 right) shows deviation from a straight crack. Like PVdF-HFP, the crack in filled PSF is scattered on the

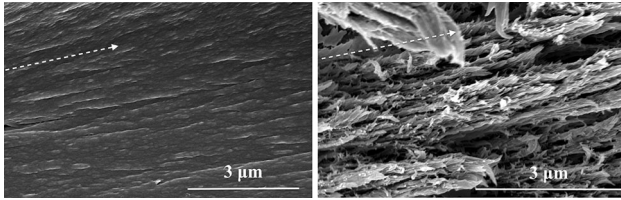


Figure 6 Fracture surface of PSF (left) and PSF/15 % CNC (right). Arrows show the crack propagation direction.

fracture surface, but unlike PVdF-HFP, the fibrous structure of the fracture surface of PSF/15 % CNC suggests that some CNC fibers have pulled-out during crack propagation. Greater fiber pull-out for PSF is consistent with a slightly poorer interface in PSF/CNC compared to PVdF-HFP/CNC (based on interface modeling) and slightly reduced essential work of fracture. We could not confirm the existence of CNC pull-out on the fracture surface due to the experimental difficulty of beam sensitivity in the SEM, which prevented sufficiently high magnification to allow direct observation of CNCs.

We conclude that CNC addition to both polymers scattered crack propagation from a straight line which tended to maintain high crack propagation toughness despite loss of ductility. Comparing the two nanocomposites suggested two reasons why toughness enhancement was greater for PVdF-HFP than for PSF nanocomposites. First, modeling suggested the interface in PVdF-HFP/CNC is better than for PSF/CNC, which is consistent with SEM suggesting more fiber pull-out for PSF. Second, because PVdF-HFP density is almost 50 % higher than PSF, the PVdF-HFP/CNC composite with 15 % fibers by weight had more fibers than the comparable PSF/CNC composite. If fibers with a good interface are diverting cracks, then the PVdF-HFP/CNC composites will have more crack-diverting fibers and therefore greater potential for enhanced toughness.

Specimen thickness effects

Because it was difficult to control thickness in specimens prepared using solution casting, our specimen thicknesses ranged from 20 to 80 μm . This variation raises a concern about the best way to measure w_e , but also provides an opportunity to probe thickness dependence of that property. The EWF method for plane stress toughness limits specimen ligament lengths to the range $3t < \ell < W/3$. The high end is to minimize

edge effects and keep plastic work confined to the ligament area. The lower end is used to keep the specimens in a state of pure plane stress. Experiments show that within this range, the net stress in the ligament at peak load is constant and close to the plane stress yield strength of a double-edge notched specimen [34]. In contrast, for $\ell < 3t$, the net stress increases indicating a mixed plane stress/plane strain stress state. Saleemi and Nairn [34] further suggested that extrapolating experiments for $\ell < 3t$ to zero ligament length can determine a plane strain essential work of fracture. But the experiments here avoided that region and instead maintained all specimens within the $3t < \ell < W/3$ range. Although this approach assures a plane stress w_e , thickness dependence in w_e could obscure the results or contribute to scatter.

Despite the frequent theoretical prediction that w_e should increase with thickness [4], few experiments have been conducted. Priest and Holmes [31] studied thickness effects in steels and saw only small effects. Levita et al. [15] examined rigid PVC and saw w_e increase with thickness. To investigate the thickness effect in thin CNC films, we reanalyzed all experiments by fitting to a 3D surface representing the fracture energy as a function of both ligament length (ℓ) and thickness (t). Both theory and experiments suggest that fracture energy is linear in ℓ for constant t , but has unknown (and possibly nonlinear) dependence on t (for constant ℓ). In brief, we refit results using a 3D fracture energy equation of:

$$w_f(\ell, t) = w_e(t) + \beta w_p \ell, \quad (6)$$

where unknowns βw_p and the thickness dependence of $w_e(t)$ were determined by fitting a semiparametric regression surface to the data. This surface was linear in the ℓ dimension and had a penalized smoothing spline to fit the nonlinearity in the thickness dimension. The fitting was done with R using a generalized additive model function (the `gam()` function from the `mgcv` package [40, 42]). This function `gam()` automatically estimates the trade-off between reducing the nonlinearity of the splines and fitting the data using generalized cross-validation. Although it would be preferable to allow thickness dependence in βw_p as well, we did not have enough experiments to resolve that much detail and therefore choose to focus on thickness dependence of $w_e(t)$. Furthermore experimental observations have suggested that βw_p is

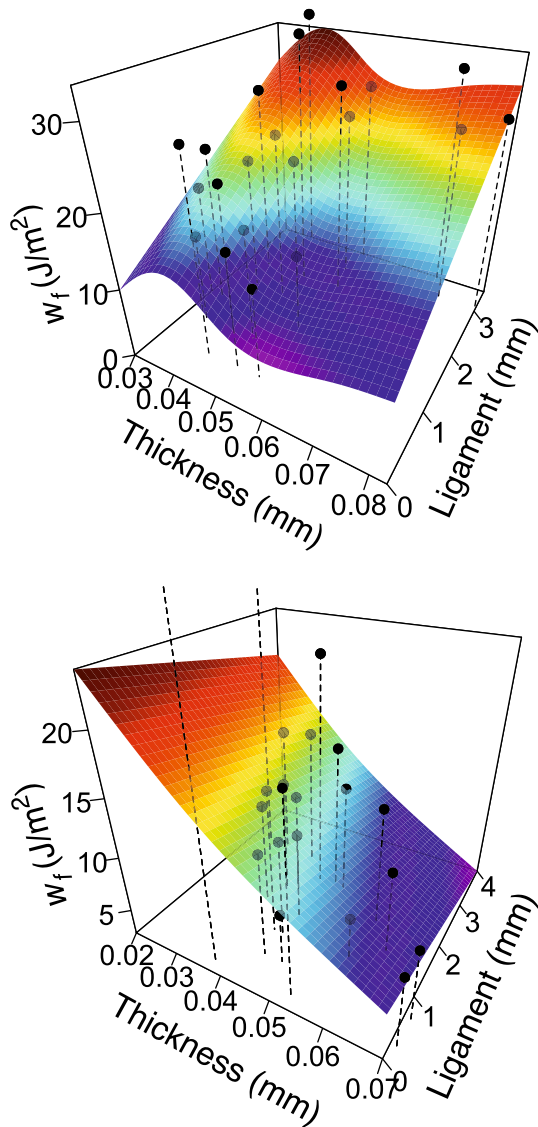


Figure 7 3D plot for the work of fracture (w_f) as a function of ligament (ℓ) and thickness in PSF (top) and for PSF/15 % CNC (bottom).

less affected by ligament stress state [34] and by thickness [15].

The fracture energy surface fits for PSF and a PSF/15 % CNC are given in Fig. 7. The dots show all experimental points. Cross sections of these plots at constant thickness show the assumed linear dependence of $w_f(\ell, t)$, but the intercepts of those lines may depend on thickness. The essential work of fracture as a function of thickness is given by the front surface of these plots (a cross section at $\ell = 0$). Figure 8 plots these $\ell = 0$ contours together with error estimates (± 1 standard error for the fit) for PSF and a PSF/15 % CNC and

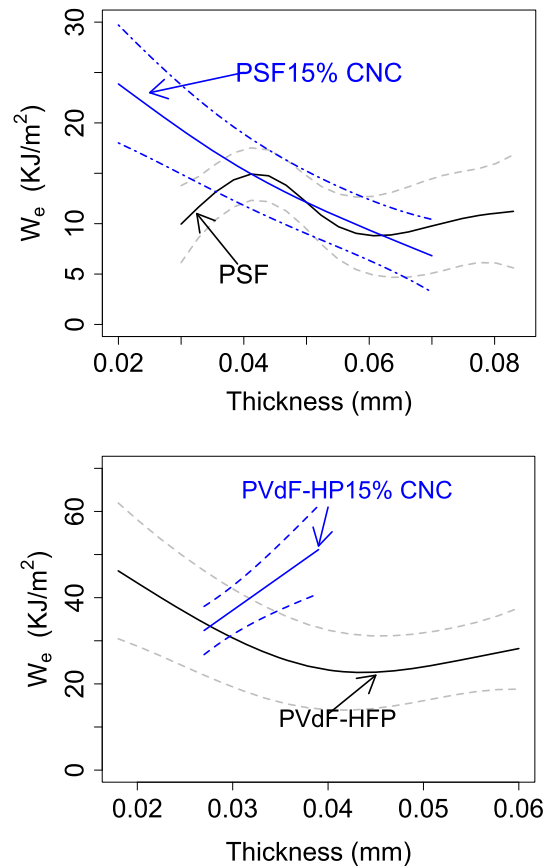


Figure 8 Extrapolation of w_f surface to zero ligament length to get w_e as a function of thickness. Top PSF and PSF/15 % CNC. Bottom PVdF-HFP and PVdF-HFP/15 % CNC. Dashed lines represent ± 1 standard error for the fit.

for PVdF-HFP and PVdF-HFP/15 % CNC. Comparing the unreinforced polymers, w_e for PSF is relatively constant, but appears to reach a peak toughness for $t = 45 \mu\text{m}$ and then decreased for thinner films. In contrast PVdF-HFP toughness increases as thickness decreases. Comparing CNC reinforced polymers to the unreinforced polymers, the w_e is always equal to or greater in the composites. This result reinforces conclusions above that adding that CNC enhances toughness when measured using crack propagation methods such as the EWFM. The two composites, however, differ in thickness dependence. The toughness of PSF/15 % CNC composites increased for thinner films while it decreased for PVdF-HFP/15 % CNC.

With the exception of the PVdF-HFP/15 % CNC results, all w_e for our thin films tended to increase as thickness decreased. This result is contrary to theoretical predictions [4] and prior experiments [15]. But the theoretical predictions are based on simplified

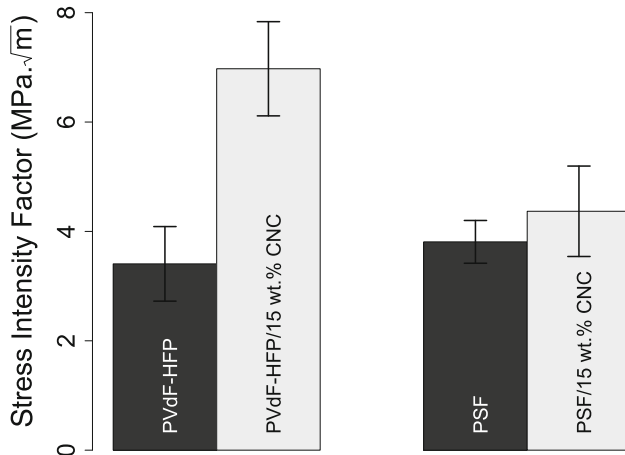


Figure 9 Toughness (K_c) for PVdF-HFP and PSF films without (dark) and with (light) 15 % CNC. The error bars represent \pm one standard deviation for confidence in the mean of specimens generated in the Monte Carlo simulation.eps.

crack opening displacement arguments that would not account for other material issues affecting fracture and the prior experiments were on much thicker films. For example, the toughness of thin titanium sheets was observed to increase or decrease with thickness depending on the crack direction and on the texture of the material [28]. Although CNC nanocomposites are not the same as titanium, our experiments suggest that alternative effects of thickness, such as texture, are more important than prior analyses based only on crack opening displacement effects.

Fracture properties

We can calculate toughness as a stress intensity factor (K_c) for our films using Eq. 2 for plane stress conditions where G_c is set equal to measured w_e . Although this calculation could be done for each film, we undertook a Monte Carlo simulation to get information about toughness and variability in toughness. In brief, we generated specimens with a range of thicknesses matching our experimental thicknesses. For each specimen the modulus was assigned randomly using the mean and standard deviation for each film and G_c was assigned randomly using the uncertainty range as a function of thickness from Fig. 8. Finally, K_c was calculated by Eq. 2 (plane stress conditions). The variability of these result values was used to estimate uncertainty in toughness.

Figure 9 shows the plane stress K_c results for all films. The stress intensity factor, K_c , shows that the

addition of 15 % CNC in PVdF-HFP increased the toughness by \sim 100 % and for PSF the toughness increased by about 16 %. These results are consistent with all previous results. The reason K_c for PSF increased slightly while w_e decreased is because the K_c calculations better accounted for thickness effects while the w_e analysis ignored thickness effects. By both methods the toughness of PSF/15 % CNC retained the toughness of pure PSF (i.e., no significant degradation in toughness).

Conclusion

In the studied systems, CNC addition decreased ductility, but increased the toughness, as measured by the EWFM, or had no detrimental effect on toughness. Modeling and fractography suggested that the mechanisms for increased or retained toughness are a good fiber/matrix interface and crack scattering around fibers during crack propagation. Toughness values for these thin films depended on thickness, although the thickness variation differed from prior concepts developed for EWFM experiments.

These conclusions about toughness differ from some prior nanocomposite studies that relied on total work of fracture experiments rather than fracture mechanics methods. We showed that our films also decreased in total work of fracture, but using that property to characterize toughness may be misleading. Our claim is that EWFM experiments provide a better evaluation of material toughness.

Compliance with ethical standards

Conflict of interest The authors declare that they have no conflict of interest.

Funding This project was support, in part, by the National Science Foundation grant CMMI 1161305, the USDA Forest Products Lab under 11-JV-1111129-137, and National Institute of Food and Agriculture under McIntyre Stennis OREZ-WSE-839-U. Also, we thank Jenna Schardt for the SEM images.

Appendix

Mean-field modeling for composite properties with randomly oriented or partially aligned fibers has two steps. The first step is to find properties of a unit cell

containing aligned fibers [8, 24]. The second step is to use mean-field averaging to find properties of randomly oriented composites.

The first step will result in $E_A, E_T, \nu_A, \nu_T,$ and G_A for the five independent mechanical properties of the transversely isotropic, aligned fibers, unit cell (axial and transverse tensile moduli and Poisson ratios and axial shear modulus, respectively). E_A can be found using the recent end-capped shear lag model [24]. This model applied optimal shear lag methods [25–27] to an axisymmetric unit cell where a cylindrical fiber with radius r_f and length l_f is encased in a cylinder of matrix with radius $r_m = r_f + \Delta$ and length $l_m = l_f + 2\Delta$. In other words, the distance from the fiber side to the unit cell side (Δ) is set equal to the distance from the fiber end to the ends of the unit cell. All fiber matrix interfaces were modeled using imperfect interface parameters $r_f D_n$ and $r_f D_t$, where D_n and D_t are interface stiffnesses for normal and tangential sliding (when $D = 0$, the interface is debonded, $D = \infty$ is perfect interface, and all other values are imperfect [8]). The axial modulus from the end-capped model, E_{EC} was derived to be [24]:

$$\frac{E_2}{E_{EC}} = 1 + \left(\frac{E_f}{E_m} - 1 \right) (V_1 - V_f) + \frac{E_f V_f}{E_m V_m} \Lambda(\rho), \quad (7)$$

where E_i is modulus and V_i is volume fraction. Subscripts f and m refer to fiber and matrix, but $V_1 = r_f^2/r_m^2$ is fiber volume fraction ignoring the end caps and $E_2 = E_f V_1 + E_m (1 - V_1)$. The key function of aspect ratio (ρ) was derived to be:

$$\Lambda(\rho) = \frac{V_m \frac{E_2 \tanh(\beta_1^* \rho)}{\beta_1 \rho} + \Lambda_1(\rho)}{V_2 \left(1 + \frac{\tanh(\beta_1^* \rho)}{\beta_1 \eta} + \frac{E_2 \tanh(\beta_2 \rho)}{\eta E_f \beta_2} \right)}, \quad (8)$$

where $\beta_1^* = (V_1 - V_f)\beta_1/(2V_f)$, $\eta = E_m V_2/(r_f D_n)$,

$$\Lambda_1(\rho) = \left(1 + \left(1 - \frac{E_2}{E_f} \right)^2 \frac{\tanh(\beta_1^* \rho)}{\beta_1 \eta} \right) \frac{\tanh(\beta_2 \rho)}{\beta_2 \rho} \quad (9)$$

$$\beta_1^2 = - \frac{4G_m V_2}{E_m (V_2 + \ln V_1)} \quad (10)$$

$$\beta_2^2 = \frac{\frac{4E_2}{E_f E_m}}{\frac{V_2}{2G_f} - \frac{1}{G_m} \left(\frac{V_2}{2} + 1 + \frac{\ln V_1}{V_2} \right) + \frac{2V_2}{r_f D_t}} \quad (11)$$

Although numerical calculations [24] show that the end-capped shear lag model is very accurate when the fiber to matrix modulus ratio, $R = E_f/E_m$, is less than 100, those calculations also show the model

becomes a lower bound for large R . This inaccuracy is not caused by shear lag methods, because all other models, including finite element models, also degenerate to lower bound results for soft matrices [24]. Because our CNCs with PVdF-HFP had $R = 190$, we introduce a correction term to model composites with soft matrices. When $R > 100$, we propose the axial modulus to be

$$E^* = \phi_L E_{EC} + (1 - \phi_L) E_{UB} \quad (0 < \phi_L < 1), \quad (12)$$

where

$$E_{UB} = \eta_f E_f V_f + E_m V_m \quad (13)$$

here E_{UB} is an “upper bound” modulus derived using fiber effectiveness methods advocated in several text books [11], where η_f is found by comparing average stress in a short fiber to the average stress that fiber would have in a continuous fiber composite:

$$\eta_f = \frac{1}{l_f \sigma_\infty} \int_{-l_f/2}^{l_f/2} \sigma_f(x) dx, \quad (14)$$

where l_f is fiber length, σ_∞ is stress the fiber would have for infinitely long fibers, and $\sigma_f(x)$ is average stress in the fiber cross section at position x . Evaluating this integral using the end-capped shear lag stress with imperfect interfaces (rather than the simplistic shear lag used in textbooks [11]) gives

$$\eta_f = 1 - \frac{1 + \left(1 - \frac{E_2}{E_f} \right) \frac{\tanh(\beta_1^* \rho)}{\beta_1 \eta} \tanh(\beta_2 \rho)}{1 + \frac{\tanh(\beta_1^* \rho)}{\beta_1 \eta} + \frac{E_2 \tanh(\beta_2 \rho)}{\eta E_f \beta_2} \beta_2 \rho} \quad (15)$$

For PSF/CNC nanocomposites ($R < 100$), the end-capped shear lag model can be used directly. For PVdF-HFP/CNC nanocomposites ($R \geq 190$), the model including both E_{EC} and E_{UB} was needed. The only remaining issue is to choose ϕ_L . We choose $\phi_L = 0.93$ based on comparing Eq. (12) to numerical results in Nairn and Shir Mohammadi [24]. This value of $\phi_L = 0.93$ appears to fit a wide range of nanocomposites when the matrix is much more compliant than the fibers.

The end-capped shear lag model gives E_A as a function of aspect ratio and interface, but mean-field modeling needs $E_T, \nu_A, \nu_T,$ and G_A as well. Fortunately, both numerical [24] and analytical [2] modeling shows that all other properties are only weakly dependent on aspect ratio. Assuming they are independent of aspect ratio, they can be found for any aspect ratio, such as for continuous fiber composites.

All remaining unit cell properties therefore used the Hashin's analysis [8] for properties of a continuous fiber composite including effects of imperfect interfaces.

The final step is to use mean-field methods for averaging unit cell properties. Here we assumed the nanocomposite films are statistically isotropic in the plane of the film (i.e., fibers tend to lie in the plane of the film). For this special case, an upper bound modulus can be found from unit cell properties using [22]:

$$E_c \leq 4U_2 \left(1 - \frac{U_2}{U_1} \right) \quad (16)$$

$$U_1 = \frac{E_A(3 + 2\nu'_A) + 3E_T + 4G_A(1 - \nu_A\nu'_A)}{8(1 - \nu_A\nu'_A)} \quad (17)$$

$$U_2 = \frac{E_A(1 - 2\nu'_A) + E_T + 4G_A(1 - \nu_A\nu'_A)}{8(1 - \nu_A\nu'_A)}, \quad (18)$$

where $\nu'_A = \nu_A E_T / E_A$ and ν_T is not needed.

References

- Anderson T, Anderson T (2005) Fracture mechanics: fundamentals and applications, 3rd edn. CRC Press, Boca Raton
- Christenson RM (1979) Mechanics of composite materials. Wiley, New York
- Cotterell B, Chia J, Hbaieb K (2007) Fracture mechanisms and fracture toughness in semicrystalline polymer nanocomposites. *Eng Fract Mech* 74(7):1054–1078
- Cotterell B, Reddell JK (1977) The essential work of plane stress ductile fracture. *Int J Fract Mech* 13:267–277
- Farshid B, Lalwani G, ShirMohammadi M, Simonsen J, Sitharaman B (2015) Boron nitride nanotubes and nanoplatelets as reinforcing agents of polymeric matrices for bone tissue engineering. *J Biomed Mater Res: Part B—Appl Biomater*
- Gojny F, Wichmann M, Köpke U, Fiedler B, Schulte K (2004) Carbon nanotube-reinforced epoxy-composites: enhanced stiffness and fracture toughness at low nanotube content. *Compos Sci Technol* 64(15):2363–2371
- Gopalan Nair K, Dufresne A, Gandini A, Belgacem MN (2003) Crab shell chitin whiskers reinforced natural rubber nanocomposites. 3. effect of chemical modification of chitin whiskers. *Biomacromolecules* 4(6):1835–1842
- Hashin Z (1990) Thermoelastic properties of fiber composites with imperfect interface. *Mech Mater* 8(4):333–348
- Henriksson M, Berglund LA, Isaksson P, Lindström T, Nishino T (2008) Cellulose nanopaper structures of high toughness. *Biomacromolecules* 9(6):1579–1585
- Huang J, Keskkula H, Paul D (2004) Rubber toughening of an amorphous polyamide by functionalized SEBS copolymers: morphology and izod impact behavior. *Polymer* 45(12):4203–4215
- Hull D, Clyne T (1996) An introduction to composite materials. Cambridge University Press, Cambridge
- Jovanovic G, Atre S, Paul B, Simonsen J, Remcho V, Chang C (2012) Microfluidic devices, particularly filtration devices comprising polymeric membranes, and method for their manufacture and use. US Patent 8,137,554
- Kelley J, Simonsen J, Ding J (2013) Poly(vinylidene fluoride-co-hexafluoropropylene) nanocomposites incorporating cellulose nanocrystals with potential applications in lithium ion batteries. *J Appl Polym Sci* 127(1):487–493
- Labour T, Vigier G, Séguéla R, Gauthier C, Orange G, Bomal Y (2002) Influence of the β -crystalline phase on the mechanical properties of unfilled and calcium carbonate-filled polypropylene: Ductile cracking and impact behavior. *J Polym Sci Part B Polym Phys* 40(1):31–42
- Levita G, Parisi L, Marchetti A, Bartolommei L (1996) Effects of thickness on the specific essential work of fracture of rigid PVC. *Polym Eng Sci* 36(20):2534–2541
- Lim SH, Dasari A, Yu ZZ, Mai YW, Liu S, Yong MS (2007) Fracture toughness of nylon 6/organoclay/elastomer nanocomposites. *Compos Sci Technol* 67(14):2914–2923
- Lin Y, Chen H, Chan CM, Wu J (2008) High impact toughness polypropylene/caco3 nanocomposites and the toughening mechanism. *Macromolecules* 41(23):9204–9213
- Ljungberg N, Bonini C, Bortolussi F, Boisson C, Heux L (2005) Cavallé: New nanocomposite materials reinforced with cellulose whiskers in atactic polypropylene: effect of surface and dispersion characteristics. *Biomacromolecules* 6(5):2732–2739
- Mai YW, Cotterell B (1986) On the essential work of ductile fracture in polymers. *Int J Fract* 32:105–125
- Mai YW, Cotterell B, Horlyck R, Visna G (1987) The essential work of plane stress ductile fracture of linear polyethylene. *Polym Eng Sci* 27:804–809
- Matsumoto N, Nairn JA (2009) The fracture toughness of medium density fiberboard (mdf) including the effects of fiber bridging and crack-plane interference. *Eng Fract Mech* 76(18):2748–2757
- Moon RJ, Martini A, Nairn J, Simonsen J, Youngblood J (2011) Cellulose nanomaterials review: structure, properties and nanocomposites. *Chem Soc Rev* 40:3941–3994
- Rusli R, Eichhorn SJ (2008) Determination of the stiffness of cellulose nanowhiskers and the fiber-matrix interface in a nanocomposite using Raman spectroscopy. *Appl Phys Lett* 93:033111
- Nairn J, Mohammadi MS (2015) Numerical and analytical modeling of aligned short fiber composites including

- imperfect interfaces. *Compos Part A Appl Sci Manuf* 77:26–36
- [25] Nairn JA (1997) On the use of shear-lag methods for analysis of stress transfer in unidirectional composites. *Mech Mater* 26:63–80
- [26] Nairn JA (2004) Generalized shear-lag analysis including imperfect interfaces. *Adv Compos Lett* 13:263–274
- [27] Nairn JA, Mendels DA (2001) On the use of planar shear-lag methods for stress-transfer analysis of multilayered composites. *Mech Mater* 33:335–362
- [28] Nasiri-Abarbekoh H, Ekrami A, Ziaei-Moayyed AA (2013) Effects of thickness and texture on mechanical properties anisotropy of commercially pure titanium thin sheets. *Mater Design* 44:528–534
- [29] Paipetis A, Galiotis C, Liu YC, Nairn JA (1999) Stress transfer from the matrix to the fibre in a fragmentation test: Raman experiments and analytical modeling. *J Compos Mater* 33(4):377–399
- [30] Pei A, Malho JM, Ruokolainen J, Zhou Q, Berglund LA (2011) Strong nanocomposite reinforcement effects in polyurethane elastomer with low volume fraction of cellulose nanocrystals. *Macromolecules* 44(11):4422–4427
- [31] Priest AH, Holmes B (1981) A multi-test piece approach to the fracture characterization of linepipe steels. *Int J Fract* 17(3):277–299
- [32] Ragosta G, Abbate M, Musto P, Scarinzi G, Mascia L (2005) Epoxy-silica particulate nanocomposites: Chemical interactions, reinforcement and fracture toughness. *Polymer* 46(23):10,506–10,516
- [33] Rink M, Andena L, Marano C (2014) The essential work of fracture in relation to j-integral. *Eng Fract Mech* 127:46–55
- [34] Saleemi AS, Nairn JA (1990) The plane-strain essential work of fracture as a measure of the fracture toughness of ductile polymers. *Polym Eng Sci* 30(4):211–218
- [35] Shah D, Maiti P, Jiang D, Batt C, Giannelis E (2005) Effect of nanoparticle mobility on toughness of polymer nanocomposites. *Adv Mater* 17(5):525–528
- [36] Shir Mohammadi M, Nairn JA (2014) Crack propagation and fracture toughness of solid balsa used for cores of sandwich composites. *J Sandw Struct Mater* 16(1):22–41
- [37] Shir Mohammadi M, Nairn JA (2016) Mean-field modeling of soft-fiber composites with imperfect interfaces and soft matrices (in preparation).
- [38] Siqueira G, Bras J, Dufresne A (2009) Cellulose whiskers versus microfibrils: Influence of the nature of the nanoparticle and its surface functionalization on the thermal and mechanical properties of nanocomposites. *Biomacromolecules* 10(2):425–432
- [39] Svagan AJ, Azizi Samir MAS, Berglund LA (2007) Biomimetic polysaccharide nanocomposites of high cellulose content and high toughness. *Biomacromolecules* 8(8):2556–2563
- [40] Team RC (2014) R: a language and environment for statistical computing. R Foundation for Statistical Computing, Vienna
- [41] Wichmann MH, Schulte K, Wagner HD (2008) On nanocomposite toughness. *Compos Sci Technol* 68(1):329–331
- [42] Wood S (2015) mgcv: mixed GAM computation vehicle with GCV/AIC/REML smoothness estimation. R package version. pp. 1.8–6